

Search for Sc_3XB ($\text{X}=\text{In, Tl, Ga, Al}$) perovskite superconductors and proximity of weak ferromagnetism.

B. Wiendlocha, J. Tobola,* and S. Kaprzyk

Faculty of Physics and Applied Computer Science,

AGH University of Science and Technology, al. Mickiewicza 30, 30-059 Krakow, Poland

(Dated: December 2, 2024)

We present results of electronic structure calculations for intermetallic perovskites Sc_3XB ($\text{X} = \text{In, Tl, Ga, Al}$) with Full-Potential KKR-LDA method. All these materials are predicted to be very promising candidates for new superconductors (related to MgCNi_3) and can be regarded as a boron-inserted cubic Sc_3X . We suggest that some of cubic Sc_3X can be magnetic, whereas Sc_3XB , having large DOS in the vicinity of E_F , exhibits non-magnetic ground state. Estimation of the electron-phonon coupling for Sc_3XB resulted in λ value ranging from 0.7 to 1. Furthermore, the effect of vacancy in Sc_3InB_x on critical parameters is also discussed in view of KKR-CPA method. Our theoretical results compare favorably with preliminary measurements, which established the transition temperature close to 4.5 K, with a very abrupt change in susceptibility and a correlated drop of the resistivity when cooling down¹.

PACS numbers: 74.10.+v, 74.25.Jb, 74.25.Kc, 74.62.Dh, 74.70.Ad, 75.50.Ce

I. INTRODUCTION

Discovery of the first non-oxide intermetallic perovskite superconductor MgCNi_3 ² with $T_c \simeq 8$ K was rather surprising due to large Ni contents and this compound was expected to be near ferromagnetic critical point³. Despite the magnetic instability, electron-phonon coupling (EPC) mechanism is definitely responsible for superconductivity in this material, but details are still not clear. Some experiments, like NMR t_1 relaxation time⁴ or specific heat measurements⁵, gave typical results, supporting s -wave pairing mechanism, with electron-phonon coupling constant $\lambda \sim 0.8$. In contrast, rather unconventional behaviors were observed in other experiments (e.g. increase of critical temperature with pressure^{6,7}, interesting properties upon doping with transition elements⁶, zero-bias conductance peak⁸ or unusual low-temperature behavior of London penetration depth $\lambda_L(T)$ ⁹), which can be partly connected with spin fluctuations likely appearing due to vicinity of ferromagnetism. Moreover, complex dynamical properties of this superconductor, as soft-mode behavior and instability of Ni vibrations^{10,11}, make theoretical analysis of MgCNi_3 quite cumbersome. Reported preliminary theoretical value of the EPC constant $\lambda \simeq 1.5$ derived from the LMTO calculations¹⁰ is higher than that extracted from specific heat jump, but consistent with thermopower measurements¹².

Among other intermetallic perovskites, related to MgCNi_3 , no new superconductor has been found so far. Systematic experimental study¹³ showed some indications of superconductivity in CaB_xPd_3 ($T_c \sim 1$ K) and NbB_xRh_3 ($T_c \sim 6$ K), but the superconducting phase was finally not identified. In spite of very similar electronic structure, no evidence of superconductivity was also found in ZnCNi_3 ¹⁴, where the effect of possible carbon deficiency was proposed as an explanation¹⁵.

In this paper we report on predictions of supercon-

ductivity in Sc_3InB compound and related isoelectronic Sc_3XB with $\text{X} = \text{Tl, Ga and Al}$. The synthesis of In- and Tl-containing cubic perovskites (space group $\text{Pm}-3\text{m}$, CaTiO_3 type) were already reported¹⁶, while Ga- and Al-containing compounds are hypothetical. Interestingly, few of these compounds seem to be also close to ferromagnetic border: Sc_3InB may be regarded as a boron-inserted cubic Sc_3In , which is a high-pressure allotropic form of the well-known hexagonal weak ferromagnet Sc_3In ¹⁷. We predict that the cubic Sc_3In is magnetic like the hexagonal phase. For other cubic Sc_3X compounds the results of electronic structure calculations are also presented, although we are not aware of the existence of these compounds.

The preliminary account for this work including superconductivity prediction and analysis of possible competition between superconductivity (Sc_3InB) and magnetism (Sc_3In) has been partly presented in the conference paper¹.

II. CALCULATIONS

We used the full-potential KKR-method, which formalism is widely discussed by many authors¹⁸, with technical details shown when applying it to Si ¹⁹. In our computations we implemented the novel quasi-linear algorithm²⁰, which allows for more precise and less time consuming band structure calculations, comparing to conventional techniques. The crystal potential was constructed within the local density approximation (LDA) and von Barth-Hedin formula was used for the exchange-correlation part. For all calculations angular-momentum cut-off $l_{max} = 3$ was set. Highly converged results were obtained for ~ 120 special \mathbf{k} -points grid in the irreducible part of Brillouin zone (IR BZ) but they were also checked for convergence using more dense \mathbf{k} -mesh. Electronic densities of states (DOS) were computed using a tetra-

hedron \mathbf{k} -space integration technique, using up to 700 small tetrahedrons.

To estimate the electron–phonon coupling strength, the EPC constant λ was calculated, using well-known equation:

$$\lambda = \sum_i \frac{\eta_i}{M_i \langle \omega_i^2 \rangle} = \sum_i \lambda_i \quad (1)$$

where i corresponds to atoms in the unit cell. This formula was originally derived by McMillan²¹ for monoatomic structures. Electronic part of the EPC constant – McMillan–Hopfield parameters η ^{21,22} were calculated for all inequivalent atoms in the unit cell using Rigid Muffin Tin Approximation (RMTA) and Gaspari–Györffy formulas²³ (see also Pickett²⁴):

$$\eta = \sum_l \frac{(2l+2)n_l(E_F)n_{l+1}(E_F)}{(2l+1)(2l+3)n(E_F)} \left| \int_0^{R_{MT}} r^2 R_l \frac{dV}{dr} R_{l+1} \right|^2. \quad (2)$$

$V(r)$ is the self-consistent potential on given atom site, R_{MT} is the site muffin–tin radius, $R_l(r)$ is a regular solution of the radial Schrödinger equation (normalized to unity in the MT sphere), and n_l is the l -th partial DOS on the site considered.

The phonon part – $\langle \omega^2 \rangle$ parameter – was derived from phonon density of states $F(\omega)$ (for discussion of applied approximations and RMTA see below). The phonon DOS was calculated using the PWscf package²⁵, where the plane wave pseudopotential technique was implemented.

A. Predictions of superconductivity in Sc_3XB

1. Sc_3InB

As we have mentioned, Sc_3InB was reported to crystallize in a perovskite structure with lattice constant $a = 4.56 \text{ \AA}$. From chemical point of view and comparing with other intermetallic perovskites, one can expect that boron (the smallest atom) should occupy the middle of the cube whereas indium should be located in its corner. However, possibility of In/B antisite defects, likely connected with the same number of valence electrons in B and In, has been reported^{1,16}. Another problem occurring in real intermetallic perovskite borides (and carbides) is related to not fully occupied boron (carbon) position. Note that various boron and carbon deficiency was observed in many related perovskites¹³, as well as in MgC_xNi_3 , where T_c decreased linearly with C concentration²⁶, and superconductivity disappeared for $x < 0.9$. The vacancy on B-site is highly plausible in Sc_3InB and this effect should be taken into account in our analysis.

Electronic structure calculations were performed with the experimental lattice constant and atomic positions: In: 1a $(0, 0, 0)$, B: 1b $(\frac{1}{2}, \frac{1}{2}, \frac{1}{2})$ and Sc: 3c $(0, \frac{1}{2}, \frac{1}{2})$. Effects of a vacancy on B-site and partly a B/In antisite disorder

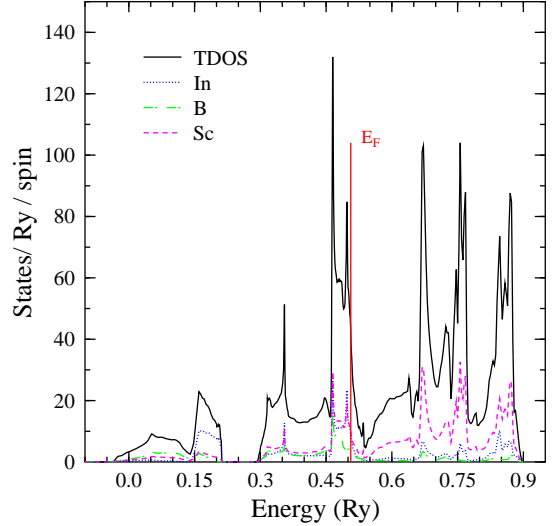


FIG. 1: KKR electronic density of states in Sc_3InB . As depicted in legends total and site-decomposed Sc (in magenta), B (in green) and In (in blue) contributions are plotted by solid and dashed lines, respectively. The Fermi level is marked by a vertical line (in red).

are discussed latter. We have employed the following *muffin–tin* spheres: $r_{MT} = 2.62$ Bohr (1 Bohr = 0.529 \AA) for Sc and In, while $r_{MT} = 1.45$ Bohr for B. From Eq. 2 we can see, that McMillan–Hopfield parameter may be sensitive to a choice of r_{MT} , so we have also checked the influence of the computational geometry on final results. The *MT* spheres variation by 15% changed the results no more than 5%.

Figure 1 presents DOS in Sc_3InB compound. The

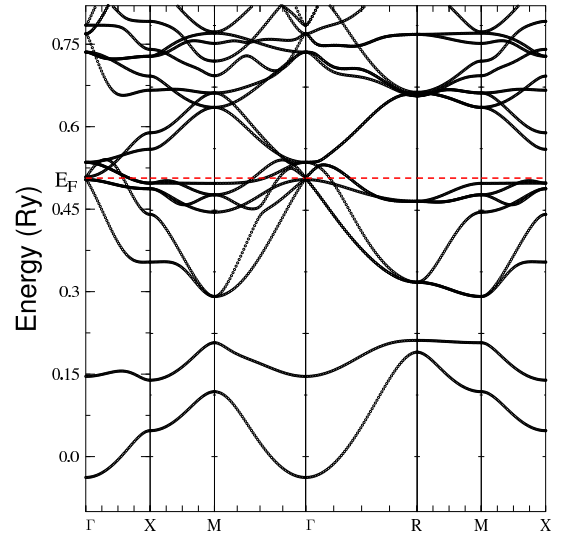


FIG. 2: Electronic dispersion curves $E(\mathbf{k})$ along high symmetry directions in Sc_3InB perovskite. The Fermi level is marked by a horizontal dashed line (in red).

Fermi level (E_F) is located on the decreasing slope of large DOS peak with the $n(E_F)$ value as large as $\simeq 90 \text{ Ry}^{-1}$. The main contributions to $n(E_F)$ can be attributed to Sc (d -states) and next In (p -states). The values of $n(E_F)$ are presented in Tab. I. Noteworthy, appearance of a large van Hove singularity close to E_F , coming essentially from transition metal d states, was also characteristic of electronic structure of $\text{MgCNi}_3^{27,28}$. The contribution from C was less important, whereas that of Mg was negligible. But Sc_3InB is a somewhat different case, since In plays more active role in forming the band structure near E_F due to presence of one electron on p -shell. The large and broad DOS peak below E_F is formed from Sc d -states hybridized with p -states from B and In. It comes from flat bands, which are well seen in $E(\mathbf{k})$ along the X – M – Γ directions (Fig. 2). Generally the bands in Sc_3InB are more dispersive comparing e.g. to MgCNi_3 or Sc_3In (Fig. 9, see below for discussion). Two separated, lowest lying bands are formed from s -states of In and B atoms, with notably large contribution from Sc. They are filled with 4 electrons: one from B and In, and two from Sc. Similar separated one band was present in MgCNi_3 , but being formed only from carbon and nickel orbitals. Ten electrons from In are confined in semi-core $4d$ -shell, which is located about 1 Ry below E_F (not shown).

Phonon calculations were undertaken for realistic approximation of $\langle \omega^2 \rangle$ in Eq. 2 within the framework of the DFPT pseudopotential technique^{25,29}. For Sc and B atoms ultrasoft pseudopotentials³⁰ were used, while for In atom norm-conserving pseudopotential was employed. LDA parameterization of Perdew and Zunger was used, all pseudopotentials included nonlinear core corrections. Plane-wave kinetic energy and charge density cut-offs were set to 35 Ry and 350 Ry, respectively. In pseudopotential calculations of electronic structure, BZ integration smearing technique of Methfessel and Paxton³¹ (with parameter $\sigma = 0.02 \text{ Ry}$) was used. The lattice constant was optimized from total energy calculations to $a_0 = 8.610(5)$ Bohr, which perfectly agrees with the experimental value ($a = 8.618$ Bohr). In order to obtain the phonon DOS, first the dynamical matrices on (5,5,5) \mathbf{q} point grid were calculated. Then, using Fourier transformation on the same grid, real-space interatomic force constants were computed. Final result – phonon density of states – was calculated by interpolating the dynamical matrices on (10,10,10) grid and using the tetrahedron method.

The phonon spectrum in Sc_3InB (Fig. 3), as one can expect from the large atomic mass differences in the unit cell, may be analyzed by dividing it into two parts. The high-frequency part of phonon DOS includes essentially vibrational modes of light B (above 50 meV). The rest – lower-frequency part of DOS (below 50 meV) contains predominantly In and Sc modes with an important peak at 13 meV coming from flat acoustic bands (mainly In vibrations). Note that similar separation in the phonon DOS was observed experimentally in MgCNi_3^{11} .

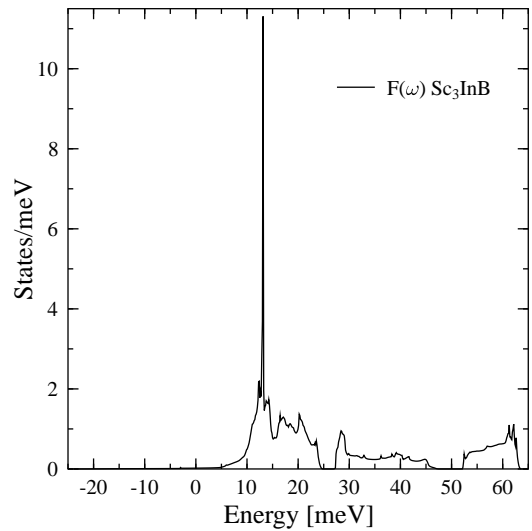


FIG. 3: Phonon density of states in Sc_3InB perovskite.

Let us remark that in our phonon calculations we met some problems with imaginary frequencies appearing near the BZ center (Γ point), which corresponded to three optical modes. At Γ point only Sc atoms vibrated in these modes, with eigenvectors lying in the three unit cell planes, being perpendicular to the Sc–C bonds. On the whole the occurrence of imaginary frequencies may indicate either the instability of the perfect perovskite structure (favoring crystal structure distortion) or an importance of anharmonic effects.

Similarly, unstable phonon branches were previously detected in $\text{MgCNi}_3^{10,11}$, but they occurred at different high-symmetry points and covered much larger volume of reciprocal space, than we have obtained in Sc_3InB . In that compound, unstable phonons corresponded mainly to anharmonic Ni vibrations, resulted from a double-well potential^{10,11,32}, in which Ni was placed. However, due to the shallowness of the double well, no stable long-range structural distortion was found there, and the perovskite structure was stabilized dynamically. The origin of unstable vibrations in Sc_3InB is appealing problem itself, but more detailed analysis of dynamical properties of the compound is out of the scope of the paper. In summary, the influence of negative frequency range on phonon density of states is rather negligible (Fig. 3), since the related energy bands are very strongly dispersive. The total weight of the unstable area is about 0.5% and should not affect calculation of $\langle \omega_i^2 \rangle$. Having phonon DOS we may proceed to estimate EPC strength.

First-principle calculations of the superconducting parameters, due to the subtle nature of such phenomenon, are still challenging problem in DFT-based computations. McMillan²¹ in his fundamental work showed, that EPC calculations may be decoupled into electronic and phonon contributions, when using few approximations. The electronic part, which describes the response of elec-

TABLE I: Properties of Sc_3InB . $n(E_F)$ is given in states/Ry/atom, η in mRy/Bohr²/atom, ω in meV, $M\langle\omega^2\rangle$ in mRy/Bohr².

Atom	$n(E_F)$	$n_s(E_F)$	$n_p(E_F)$	$n_d(E_F)$	$n_f(E_F)$	η	η_{sp}	η_{pd}	η_{df}	$\sqrt{\langle\omega^2\rangle}$	$M\langle\omega^2\rangle$	λ
Sc	20.26	0.06	2.34	16.98	0.88	18.6	0.0	4.7	13.3	18.5	75.7	0.74
In	18.28	0.04	16.72	1.16	0.32	1.5	0.0	1.5	0.0	18.5	193.4	0.01
B	6.72	0.02	5.92	0.42	0.36	34.3	0.0	34.3	0.0	58.3	180.9	0.19

trons from Fermi surface to displacements of atoms, is most often computed with Gaspari–Györffy method²³, which usually involves three main assumptions³³:

- (i) *rigid-ion approximation*, in which potential inside the MT sphere moves rigidly with the ion and the change in crystal potential, caused by the displacement, is given by the potential gradient;
- (ii) *local-vibration approximation*, which neglects the off-diagonal terms in Eq. 1. More generally $\lambda = \sum_{ij} \lambda_{ij}$, where (i, j) refer to two (generally different) atoms in the unit cell, for $\lambda_{ij} = \delta_{ij} \lambda_i$ it yields Eq. 1;
- (iii) *spherical band approximation*, which leads to only dipole ($l \rightarrow l + 1$) transitions in Eq. 2.

It is known that all mentioned assumptions work well for the transition metals and cubic-site symmetry. Conversely, in simple metals the assumptions (i) and (ii) generally underestimate EPC³⁴ due to a poorly screened crystal potential, whereas, hopefully, the corrections to (iii) are expected to be small for cubic transition metals³⁵.

Another simplification is necessary to calculate $\langle\omega^2\rangle$ in Eq. 1 using $F(\omega)$, which is so-called 'constant- α approximation' (see e.g. Butler³⁶ for discussion). This means that the electron–phonon interactions are considered to be independent of phonon frequency ω and the factor α cancels⁵⁹ when calculating $\langle\omega^2\rangle$. The assumption of the constant α is well fulfilled e.g. in niobium³⁷ but in multi-atom compounds, this remains a serious limitation, since only somewhat 'averaged' λ can be obtained.

The RMTA and Gaspari–Györffy theory has been successfully used for analyzing EPC in many superconducting materials, like pure metals³⁸, binary alloys³⁹, A –15 compounds⁴⁰, transition metal carbides^{41,42}, borocarbides⁴³ or metal–hydrogen system⁴⁴. Reasonable results (as far as λ is concerned) were usually obtained, even in such unusual superconductor as MgB_2 ⁴⁵. This formalism was helpful in discussing phonon-based effects in high-temperature superconductors^{33,46}. Certainly, in order to better understand the electron–phonon interactions in a potential superconductor one has to perform more elaborated calculations, involving Eliashberg gap equations (see for example remarkable results for MgB_2 ^{47,48}). Nevertheless, electronic structure and phonon calculations within the simplified RMTA framework seem to be reliable tools to search for new superconductors.

Based on this methodology the McMillan–Hopfield parameters were calculated for Sc_3InB (Table I). In scandium the most important is $d - f$ scattering channel,

which is typical for transition metals. Note that although the η_B value was found to be the largest in our system, η_{Sc} occurred to be more important in calculation of λ , since it should be counted three times (3 Sc atoms in unit cell). η_{In} had negligible value despite a noticeable density of states at the Fermi level.

In the calculation of mean square phonon frequencies $\langle\omega_i^2\rangle$ we had to face the latest important point of our analysis: how to get $\langle\omega_i^2\rangle$ for every atom in the complex compound from the total $F(\omega)$. Taking the same $\langle\omega_i^2\rangle$ for all atoms, what is sometimes done, may occur not appropriate⁴¹ due to disregard for atomic-like character of η ($M\omega^2$ corresponding to an effective force constant is also a site-dependent quantity). In compounds, where atoms have markedly different masses, the lightest atom would be favored in the way, as shown below. The mean phonon frequencies were computed according to the above-mentioned analysis of the phonon DOS with separation energy of about 50 meV. $\langle\omega_i^2\rangle$ for In and Sc were calculated from lower-frequency part of the spectrum and were taken the same for both atoms. The average $\langle\omega_B^2\rangle$ was computed from the high-frequency part of DOS and resulted in significantly larger value, which reflects small mass of B (see Tab. I).

Total electron–phonon coupling constant is $\lambda = 0.94$ with the main contribution from Sc. Using McMillan formula for critical temperature and applying a typical value of Coulomb pseudopotential $\mu^* = 0.13$, we estimated $T_c \simeq 12$ K⁶⁰. Both calculated λ and T_c values belong to a moderate regime of superconducting parameters within the RMTA model, and are even higher than those in MgCNi_3 . We have also verified how our results might change when $\langle\omega^2\rangle$ was taken to be equal for all atoms. We have obtained $\lambda = 1.6$ with $\lambda_B = 1.1$ and $\lambda_{Sc} = 0.5$ when employing $\sqrt{\langle\omega^2\rangle} = 23.4$ meV, as derived from the whole phonon spectrum. The resulting critical temperature $T_c = 26$ K was two times larger than the previously estimated value, and probably much overestimated, due to the overestimation of boron contribution.

Furthermore, we can notice advantageous tendency of electron–phonon coupling in Sc_3InB comparing with MgCNi_3 superconductor. Our KKR calculations for MgCNi_3 showed that Ni had the largest McMillan–Hopfield parameter: $\eta_{Ni} = 20$ mRy/Bohr², with respect to other atoms ($\eta_C = 9$ mRy/Bohr², η_{Mg} – a negligible value). The value of η_{Sc} in Sc_3InB is similar to η_{Ni} in MgCNi_3 but η_B is over three times larger than η_C . In view of recent C isotope effect measurements⁴⁹ (i.e. very large $\alpha_C = 0.54$ coefficient) and bearing in mind a

particular sensitivity of T_c on the carbon concentration, one can conclude that both C and Ni sublattices are important in superconductivity of MgCNi_3 . In view of this criterion T_c in Sc_3InB can be expected even higher than in MgCNi_3 .

Pressure effect on electronic properties of Sc_3InB was also examined by varying lattice parameter in KKR computations. In spite of $n(E_F)$ decrease with volume contraction: $dn(E_F)/dV = 0.42$, McMillan–Hopfield parameters increased for all atoms, with quite typical ratio, namely: $d\ln\eta_B/d\ln V = -2$, $d\ln\eta_{Sc}/d\ln V = -1.5$ and $d\ln\eta_{In}/d\ln V = -2.4$. This result suggests, that external pressure may enhance T_c , as observed in MgCNi_3 ^{6,7}, but of course the effect of lattice stiffening may be dominant.

Effect of nonstoichiometry

A deficiency on light element site (B, C), often observed in real perovskite samples, have prompted us to perform the calculations of electronic structure and McMillan parameters in Sc_3InB_x and MgNi_3C_x from the *muffin-tin* KKR–CPA method⁵⁰.

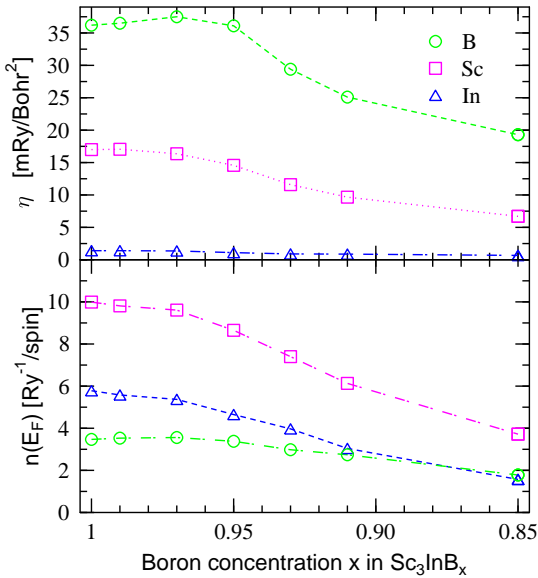


FIG. 4: Effect of B–sublattice deficiency in Sc_3InB_x on site-decomposed McMillan–Hopfield parameters (upper panel) and corresponding DOS at the Fermi level computed from KKR–CPA method (see text). In both panels, the corresponding values for Sc (in magenta), B (in green), and In (in blue) are marked by squares, circles and triangles, respectively. Lines connecting calculated points are added as a guide to the eye.

At a first glance one observes that all site contributions to DOS at E_F significantly decreased in Sc_3InB_x with the decrease of boron concentration from 1 to 0.85 (Fig. 4), which is in contrast to the rigid–band expectations. De-

tailed analysis of KKR–CPA DOS in Sc_3InB_x (see also Fig. 10) indicated that a vacancy on B–site seems to behave as a hole donor (if the pseudo gap in DOS found above E_F can be considered as a separation between valence–like and conduction–like bands). Since the potential of the vacancy is much more repulsive than the potential of B atom, all p –states (accommodating 6 electrons) were expelled into higher energy (well above E_F) against only 1 electron occupying p –shell in B atom. Consequently, the filling of low–lying conduction–like states decrease when the vacancy concentration increased.

From detailed analysis of critical parameters in the small vacancy range (B concentration $1 < x < 0.85$) we have found a significant change in the η value for Sc and (less important) for B. This strongly affects the EPC parameter, i.e. for 7% boron deficiency, using the values of $\langle\omega_i^2\rangle$ obtained in the stoichiometric compound, total λ decreased over 30% to $\lambda \simeq 0.6$, which resulted in three times lower critical temperature: $T_c \simeq 4$ K. When vacancy concentration reached 15% (i.e. $\text{Sc}_3\text{InB}_{0.85}$) superconductivity was practically quenched, since the coupling constant became very small ($\lambda \simeq 0.4$).

This behavior seems to be similar to MgCNi_3 case, where lowering of T_c with increase of vacancy concentration was observed experimentally^{26,51}. However, from our preliminary KKR–CPA calculations of density of states for MgC_xNi_3 (for small vacancy concentration), we observed a tendency of slight increase of total DOS at the Fermi level. Hence, the evolution of the superconductivity is expected to be more complex comparing to the behaviors detected in Sc_3InB_x . The disappearance of superconductivity in MgC_xNi_3 requires more careful analysis of McMillan–Hopfield parameters accounting for possibility of spin fluctuations that may also suppress superconductivity and will be discussed elsewhere. So far it was suggested⁵¹, that there are two isostructural phases of MgC_xNi_3 : α – MgCNi_3 (for $x < 0.90$), which is not a superconductor, and superconducting β – MgCNi_3 ($x > 0.90$), with 1.2% larger lattice constant. The presence of two phases may also modify (already complicated) dynamic properties of this compound, which are equally important for superconductivity as the electronic structure.

Furthermore, following the X–ray refinements data¹ in the $\text{Sc}_3\text{In–B}$ we intended to study the antisite In/B disorder on a superconducting state. The current KKR–CPA results became only qualitative due to substantially modified computational geometry, i.e. in perfectly ordered Sc_3InB the muffin–tin radius of B was two times smaller than of In, which was no more valid when trying to compare electronic properties of exchanged atoms. We can roughly conclude that DOS and η parameters on all sites vary in complex way, depending on the magnitude of the antisite In/B disorder. Hence, precise experimental data including an evolution of lattice constant and a partial disorder on all sites in the perovskite structure are required to permit more quantitative analysis of the antisite In/B disorder on the Fermi surface parameters from

the KKR-CPA calculations.

2. Sc_3TlB , Sc_3GaB and Sc_3AlB .

Interesting properties of Sc_3InB encouraged us to investigate electronic structure along isoelectronic Sc_3XB compounds. Among these systems, only Sc_3TlB perovskite was reported¹⁶ with a lattice constant $a = 4.52 \text{ \AA}$, very close to that of Sc_3InB perovskite ($a = 4.56 \text{ \AA}$). The electronic structure of both compounds was also expected to be similar (Fig. 5).

The semi-relativistic calculations were performed in this compound due to a heavy Tl ($Z = 81$). The Fermi surface properties listed in Tab. II indicate that DOS and η parameters are close in these compounds and they do not differ considerably from Sc_3InB . Because of few similarities noticed in these compounds, i.e. very close lattice constants, alike electronic structure and distribution of atomic masses in the unit cell, one can expect that dynamical properties of Sc_3TlB and Sc_3InB should not be quite different (perhaps instead of lowering of Tl frequencies). Estimation of electron-phonon coupling constant using the previously calculated $\langle \omega_i^2 \rangle$ values (Tab. I) was partly justified. Indeed, the resulting EPC constants (Tab. II) were comparable to those computed in Sc_3InB ($\lambda = 0.95$ and $T_c \simeq 12 \text{ K}$).

Next we have investigated hypothetical Sc_3GaB taking the lattice constant of Sc_3InB . The electronic structure of the compound was also analogous to that presented in other Sc_3XB compounds (Fig. 5, Tab. II), indicating that rigid-band model favorably works in this series of compounds. However, McMillan-Hopfield parameters for Sc (lower than that in Sc_3TlB) and B (higher than that in Sc_3TlB) are slightly different (Tab. II). Since Sc played the most important role in the EPC magnitude, λ was predicted to decrease. Owing Ga is almost two times lighter than In, the criterion of atomic mass asymmetry

TABLE II: Properties of Sc_3XB . $n(E_F)$ is given in states/Ry/atom, η in mRy/Bohr²/atom, ω in meV, $M\langle \omega^2 \rangle$ in mRy/Bohr².

Atom	$n(E_F)$	η	$\sqrt{\langle \omega^2 \rangle}$	$M\langle \omega^2 \rangle$	λ
Sc	14.8	19.1	18.5 ^a	75.7	0.755
Tl	12.5	1.6	18.5 ^a	344.2	0.005
B	14.4	34.1	58.3 ^a	180.9	0.188
Sc	21.62	17.4	20 ^b	88.5	0.590
Ga	23.76	2.1	20 ^b	137.3	0.015
B	6.74	35.1	58.5 ^b	182.1	0.193
Sc	23.78	17.8	21.3	100.4	0.532
Al	26.08	1.3	21.3	60.3	0.022
B	7.08	33.4	58.6	182.7	0.181

^aapproximated from Sc_3InB values (see text).

^binterpolated between Sc_3InB and Sc_3AlB values (see text).

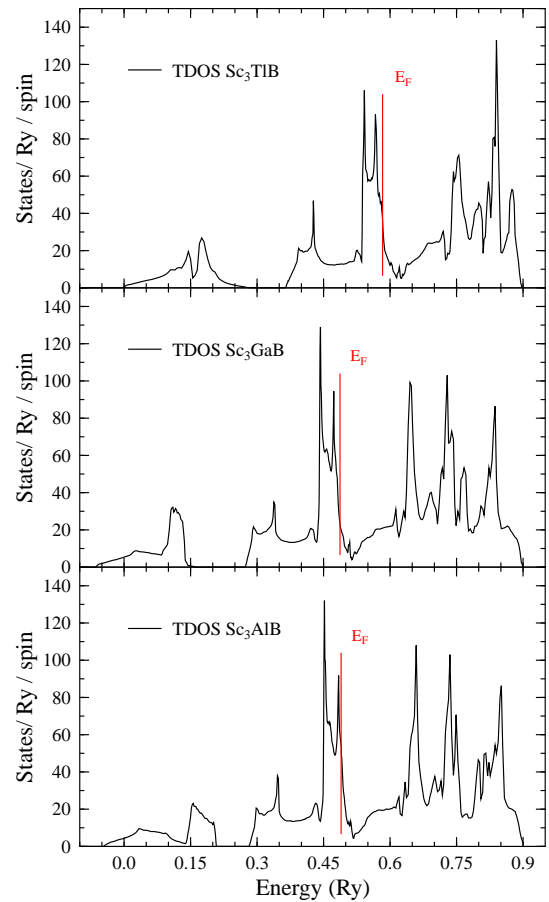


FIG. 5: KKR total DOS of isoelectronic Sc_3XB perovskites. Only Sc_3TlB ($a = 4.52 \text{ \AA}$) was reported¹⁶, whereas Sc_3GaB and Sc_3AlB remain hypothetical. The Fermi level is marked by a vertical line (in red).

that was previously used to separate atom contributions (Sc, X and B) from total phonon DOS, was less evident.

To complete our analysis along this series of compounds, Sc_3AlB was next considered. Since electron configuration of Al contains only s —an p —like orbitals, thus different from the precedent cases, where semicore d -like levels appeared, it was possible to study an effect of complete nd^{10} shell on electronic states. Total energy minimization with respect to a lattice constant gave almost the same result as in Sc_3InB : $a_0 = 8.610(5)$ Bohr. The band structure was also similar to the above-mentioned compounds, which supports widely accepted conclusion that $3d$ -Ga, $4d$ -In and $5d$ -Tl electrons form truly core-like levels, and the effect on upper lying electronic states (particularly near E_F) was small (see Fig. 5, Tab. II). Also interesting comparison can be made when investigating the X -atom effect on phonon DOS, since the range of a mass variation was quite important, i.e. from $M = 27$ (Al) to $M = 115$ (In).

Phonon DOS calculations in Sc_3AlB (Fig. 6) were performed using 30 Ry for kinetic energy wave function cut-off and norm-conserving pseudopotential for Al (the rest

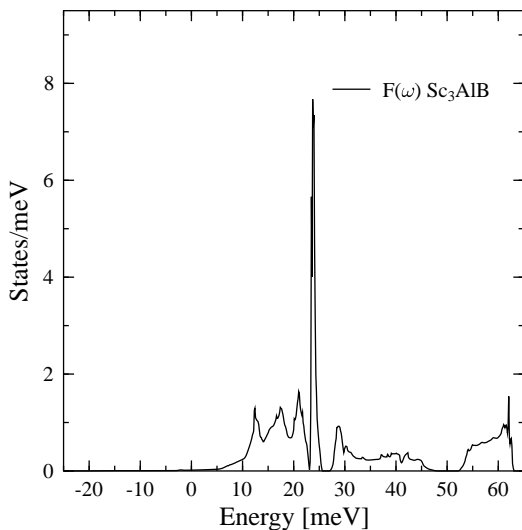


FIG. 6: Phonon density of states in hypothetical Sc_3AlB .

parameters were the same as in Sc_3InB). In spite of different distribution of atomic masses in the cell, than in Sc_3InB , $F(\omega)$ changed in more or less 'rigid-band' manner. The acoustic modes range broadened, which was manifested in a shift of their flat part from 13 meV in Sc_3InB to 25 meV in Sc_3AlB . The rest of the phonon DOS shape only slightly changed. Note that we met similar problems with unstable phonons at Γ point as in Sc_3InB , due to the same Sc optic modes.

The average phonon frequencies $\langle\omega_i^2\rangle$ were computed as in the previous section, and are slightly larger (see Tab. II). The estimated coupling constant for Sc was considerably lower because of both lower η and higher ω . The total EPC parameter was found as large as $\lambda = 0.735$, and with average frequency $\langle\omega\rangle = 22.7$ meV and $\mu^* = 0.13$ corresponded to the transition temperature $T_c \simeq 8$ K.

The 'rigid-band-like' behavior of the phonon DOS, as far as the X -atom mass variation is concerned, enabled to predict $\langle\omega_i^2\rangle$ for Sc_3GaB without direct calculations of $F(\omega)$. Since the atomic mass of Ga ($M = 70$) lies in the middle between that of In ($M = 115$) and Al ($M = 27$), so we may roughly estimate $\langle\omega^2\rangle_{\text{Sc},\text{Ga}}$ and $\langle\omega\rangle$ in Sc_3GaB interpolating the values already calculated in Sc_3InB and Sc_3AlB : $\langle\omega^2\rangle_{\text{Sc},\text{Ga}} \simeq (20 \text{ meV})^2$ and $\langle\omega\rangle \simeq 21$ meV. The average B frequency was taken to be $\langle\omega^2\rangle_B \simeq (58.5 \text{ meV})^2$, and the resulting EPC constants were similar to Sc_3AlB (Tab. II) with total $\lambda = 0.798$ and $T_C \simeq 9$ K (again $\mu^* = 0.13$ was used).

B. Magnetic properties of cubic Sc_3X

1. Sc_3In

Since all presented compounds, both existing (Sc_3InB and Sc_3TIB) and hypothetical (Sc_3GaB and Sc_3AlB), are believed to be promising candidates for superconductors, one may also ask about possible competition of superconductivity with magnetism in these systems. In MgCNi_3 such remark was quite natural due to three Ni atoms in the unit cell. Here, as above-mentioned in Sec. I, instability towards magnetism may be present because of weak ferromagnetic properties of Sc_3In . First, we have studied electronic structure of both allotropic phases of this compound. The hexagonal phase (Ni_3Sn -type with lattice constants $a = 6.42 \text{ \AA}$, $c = 5.18 \text{ \AA}$ ⁵²) is a well-known weak itinerant ferromagnet¹⁷, while the cubic form (Cu_3Au -type with a lattice constant $a = 4.46 \text{ \AA}$, synthesized under high pressure⁵³) has not been yet investigated to our knowledge.

KKR calculations were performed using experimental lattice parameters. In the Ni_3Sn -type Sc_3In , the adjustable parameter x positioning Sc atoms in the unit cell (admitted by the space group No.194) and defining the Sc-Sc distances in a hexagonal plane, was taken to have the ideal value of $x = 5/6$, following the X-ray analysis⁵² and previous calculations⁵⁴. The MT sphere radius 2.7 Bohr was used, the same for Sc and In, in hexagonal and cubic phases, since interatomic distances are also similar (other computational details as in Sec. II A).

The spin-polarised DOS, presented in Fig. 7 and Tab. III, were quite similar for both compounds. Note that in hexagonal phase there are 8 atoms in the unit cell (2 In and 6 Sc), so the total DOS at Fermi level was higher, but the scandium contributions are comparable in both phases. At first glance the DOS shape and the resulting magnetic ground state of both phases were remarkably close. Magnetic properties are due to magnetic moment on Sc atoms: $0.26 \mu_B$ (hexagonal) and $0.27 \mu_B$ (cubic) but we should remind that experimentally measured magnetic moment was much weaker, i.e. $\sim 0.05 \mu_B/\text{Sc}$ in hexagonal phase. The overestimation of magnetic moment in LDA calculations on one hand as well as a lack of saturation of experimental magnetization curves versus magnetic field on the other, are typical behaviors of weak ferromagnetism. Noteworthy, the discrepancy concerning μ value on Sc was already underlined in the LAPW calculations for hexagonal phase⁵⁴. Hence, we predicted that Sc_3In com-

TABLE III: Spin-polarised DOS of Sc_3In . $n(E_F)$ is given in states/Ry/cell, n_{Sc} in states/Ry/Sc, μ_{Sc} in μ_B .

Compound	$n_{\uparrow}(E_F)$	$n_{\downarrow}(E_F)$	$n_{\uparrow\text{Sc}}(E_F)$	$n_{\downarrow\text{Sc}}(E_F)$	μ_{Sc}
Sc_3In (cub)	60.71	30.60	17.96	9.72	0.27
Sc_3In (hex)	139.4	55.10	19.33	8.51	0.26

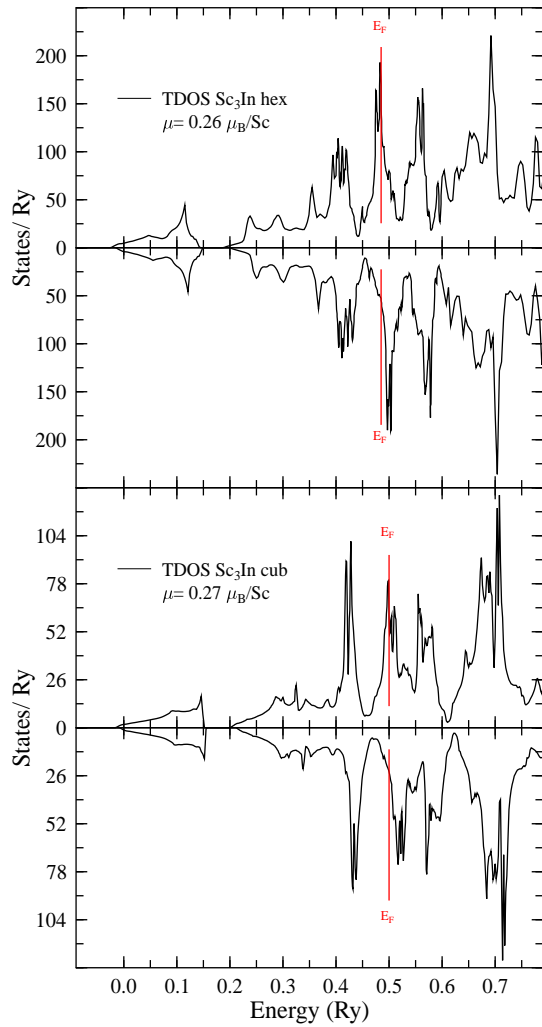


FIG. 7: KKR spin-polarised total DOS in hexagonal (Ni_3Sn -type, upper panel) and cubic (Cu_3Au -type) Sc_3In . Both compounds exhibit very close magnetic moments on Sc atoms (see text). Density of states is given per Wigner–Seitz cell and is then almost two times larger in the hexagonal form of Sc_3In , but very close on the corresponding Sc sites. The Fermi level is marked by a vertical solid line (in red).

pound may be another Cu_3Au -type weak ferromagnet, like Ni_3Al (see e.g.⁵⁵), but this theoretical result should be verified experimentally. Also we may recall that some weak ferromagnets exhibit superconducting properties (e.g. Y_9Co_7 ⁵⁶ or the most famous ZrZn_2 ⁵⁷), so the experimental re-investigation of cubic Sc_3In should be indeed very interesting. Besides, in view of the analysis of electronic structure features the weak ferromagnet-to-superconductor transition seems plausible in Sc_3InB_x if controlling the variation of the B concentration.

2. Sc_3Tl , Sc_3Ga and Sc_3Al

Within the isoelectronic Sc_3X cubic series, only the Sc_3In compound was synthesized so far. In order to have the possibility of wider comparison between the two series, electronic structure of three hypothetical structures: Sc_3Al , Sc_3Ga and Sc_3Tl were calculated. Since we are probably dealing with very weak magnetic systems, thus calculations of magnetic moments without knowledge of experimental lattice constant would be rather speculative. Hence, further analysis is based on the KKR total DOS values and Stoner factors, where the lattice constant of Sc_3In ($a = 4.46 \text{ \AA}$) was employed for all Sc_3X compounds. In Table IV we summarized the electronic structures of these compounds and the non spin-polarised DOS are presented in Fig. 8.

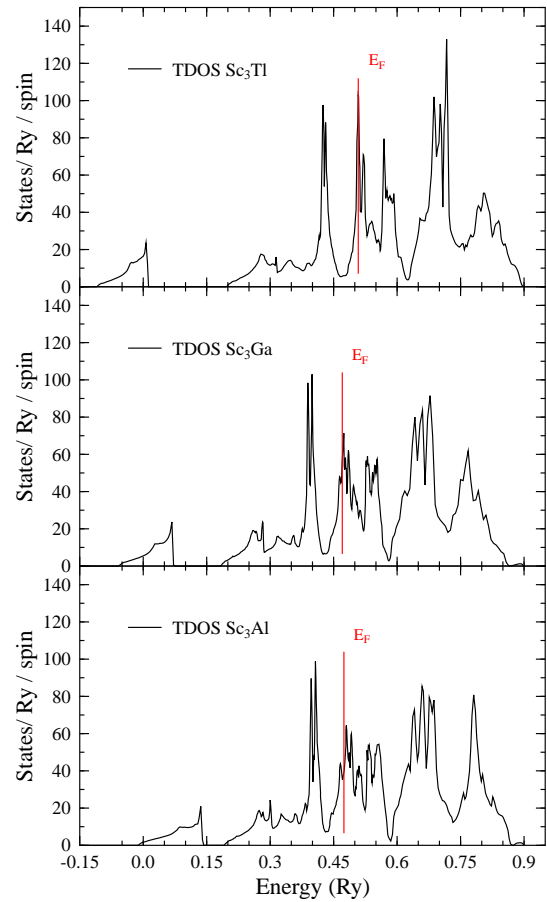


FIG. 8: KKR non-polarised total DOS in hypothetical (Cu_3Au -type) Sc_3X $X = \text{Tl}$, Ga and Al . The Fermi level is marked by a vertical line (in red).

The most evident feature of this series is monotonic decrease of the Stoner factors, with atomic number Z . For Sc_3In $In_{Sc}(E_F)$ is greater than 1, which is consistent with a magnetic ground state obtained with the spin-polarised KKR calculations. Based on Stoner theory one can expect that an appearance of ferromagnetism in

TABLE IV: Non spin-polarised DOS of Sc_3X and Stoner factors. $n(E_F)$ is given in states/Ry/cell, n_{Sc} in states/Ry/atom.

Compound	$n(E_F)$	$n_{Sc}(E_F)$	$I_{Sc}n_{Sc}(E_F)$
Sc_3Tl	205	64.90	1.89
Sc_3In (cub)	136	43.23	1.26
Sc_3Ga	112	34.72	1.03
Sc_3Al	79	23.26	0.70

Sc_3Tl , while in Sc_3Al non-magnetic ground state seems to be more favorable. Interestingly, Sc_3Ga was found near the Stoner limit.

C. Superconductivity vs. Ferromagnetism

Studying possible competition of superconductivity and weak ferromagnetism is directly related to investigation of the role of trivalent boron in the entitled compounds. To get a better insight, the KKR-CPA calculations for Sc_3InB_x (and MgC_xNi_3 for comparision) have been performed in full range of x concentration.

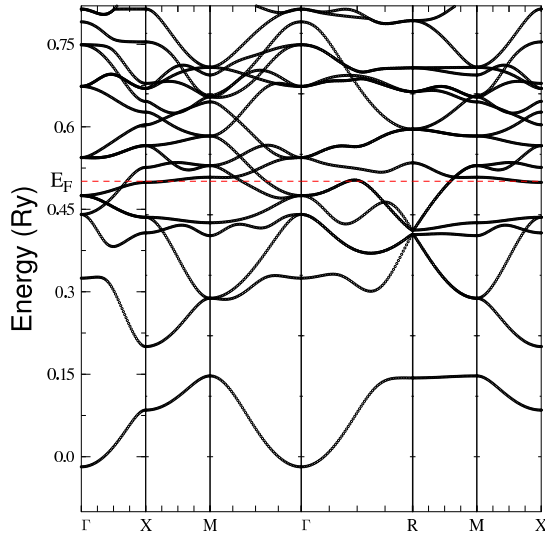


FIG. 9: The non-polarised electronic dispersion curves $E(\mathbf{k})$ along high symmetry directions in cubic Sc_3In . The Fermi level is marked by a horizontal dashed line (in red).

First, analyzing the DOS values for Sc_3In (Tab. IV) it is worth noting, that the large $n(E_F)$ value consists mainly (about 95%) of scandium atoms contribution. This gives the large Stoner factor on Sc atom and makes the magnetic ground state energetically favorable. Then, from the DOS evolution presented on Fig. 10, we observe, that when the B concentration increases, the Fermi level is shifted from the strongly increasing DOS (5% B), towards a deep valley ('pseudogap', 75% B). After crossing it, the $n(E_F)$ value again increases, and the Fermi level

is now found on the left side of the DOS valley (95% B), but here the Stoner limit is not reached. Comparing band plots of limiting cases (Sc_3In – Fig. 9 and Sc_3InB – Fig. 2) one concludes that additional hybridization occurring between B p -states and Sc d -states makes the band structure in Sc_3InB more dispersive. Looking at the DOS at Fermi level, we can also note that boron-inserted compound has considerably lower $n(E_F)$ value. Also the DOS at Fermi level on the scandium atom $n_{Sc}(E_F)$ in Sc_3InB is two times lower than that in Sc_3In and consequently the Stoner factor is only about 0.6. In addition, the scandium atoms contribution to total DOS falls to 71%. This prevents formation of magnetic ground state in Sc_3InB .

Another interesting result concerns the formation of one additional, separated lowest-lying band in Sc_3InB . In Sc_3In there is one such band, attributed to In s -orbital and Sc orbitals. Additional boron s -orbital in Sc_3InB (after hybridization with scandium) forms second band, which bounds one electron from B and one electron from Sc, which is extracted from upper-lying bands. Finally, in the main part of band region below E_F , there is one Sc electron less, comparing to Sc_3In . This may be another mechanism of lowering scandium contribution to $n(E_F)$ and preventing the ferromagnetism. Interestingly, in spite of lowering $n_{Sc}(E_F)$, McMillan–Hopfield parameter for Sc increases from ~ 13 (in Sc_3In) to ~ 19 mRy/Bohr² (in Sc_3InB), which is crucial for superconductivity onset. This is partially caused by the increase of f -states DOS near E_F (mostly n_f/n_{tot} ratio) which pushes up the η_{Sc} value in the $d-f$ transfer channel. The boron contribution to the final EPC constant λ is of course also important. All these makes the Sc_3InB a possible superconductor.

The appearance of magnetic ground state in Sc_3In makes Sc_3InB even more similar to MgC_xNi_3 , since MgC_xNi_3 was theoretically predicted to have a small magnetic moment (about $0.4 \mu_B$ per Ni atom⁵⁸). We confirmed this result from our KKR calculations, resulting in practically the same value ($\mu = 0.40 \mu_B$ per Ni atom), when assuming the same lattice contraction⁶¹, as between Sc_3InB and Sc_3In . To have a tentative comparison, similar KKR-CPA calculations for MgC_xNi_3 ($1 < x < 0$) were performed (Fig. 10). The evolution of electronic structure is quite different, since when the carbon concentration decreases, E_F moves towards lower energy (in contrast to Sc_3InB_x), crosses the DOS valley and falls into the higher-DOS region, where magnetic ground state appears. Also it is worth noting, that van Hove singularity near E_F , which was the main electronic structure feature of MgC_xNi_3 , disappears smoothly with the vacancy concentration, due to the deficiency of carbon p -orbitals.

Concluding, one can expect that the proximity of ferromagnetic quantum critical point (resulting in enhanced spin fluctuations) may probably compete with superconductivity in Sc_3InB as already was suggested in MgC_xNi_3 ^{3,10}.

Interestingly the *strength of magnetic interactions* in

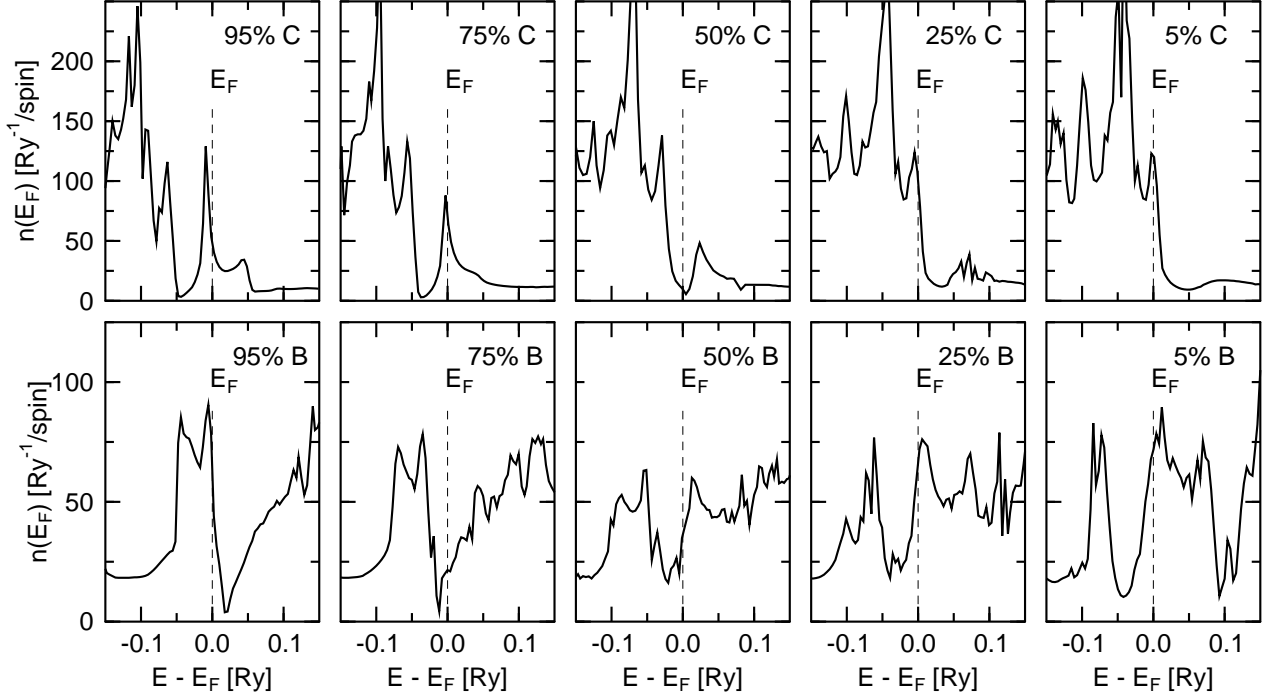


FIG. 10: Effect of vacancy on total density of states in MgC_xNi_3 (upper panels) and Sc_3InB_x from KKR-CPA calculations. Note, a remarkable evolution of electronic states in the vicinity of the Fermi level: from high DOS at E_F in C-rich and B-rich samples (left side: i.e. near full C/B occupancy and superconductivity limit) through a deep DOS minimum (intermediate concentrations, i.e. near 50% C in MgC_xNi_3 and c.a. 80% B in Sc_3InB_x) to again large DOS, which satisfy the Stoner criterion (right side, i.e. near empty C/B sublattice limit). The Fermi level is at zero (marked by a vertical dashed line) to facilitate the comparison between both series of alloys.

Sc_3X and the magnitude of the EPC constant in Sc_3XB seems to be correlated. Both the highest Stoner factor and EPC parameter λ were obtained for Tl- and In-based compounds, and are considerably lower for Ga and Al cases. Furthermore, the tendency in decreasing λ (in Sc_3XB) is *opposite* to the $n(E_F)$ modifications.

III. CONCLUSIONS

We have presented theoretical investigation of superconducting properties of the perovskite series Sc_3XB ($X = \text{In, Tl, Ga, Al}$) and their possible connections with weak magnetism in Sc_3X compounds. Our main results predicted : (i) superconductivity in Sc_3InB , with $\lambda \simeq 1$ and $T_c \simeq 12$ K; (ii) weak ferromagnetism in Sc_3In ; (iii) important effect of vacancy on electronic structure of Sc_3InB_x compound.

We have also showed, how boron insertion to the cubic Sc_3In may destroy the magnetic ground state, and likely turn the Sc_3InB system into a superconductor.

Preliminary experimental examination of the Sc_3InB system was undertaken¹, but several synthesis procedures did not succeed in preparing a single-phase and stoichiometric compound. However, one of the samples showed signs of superconductivity with $T_c \simeq 4.5$ K. This

sample consisted of two main phases: hexagonal Sc_2In (30% vol.) and cubic Sc_3InB (70% vol.), with additional vacancies (or disorder) in the perovskite phase. Unfortunately, the sample occurred to be unstable, and superconductivity disappeared after several hours in ambient atmosphere. The problems with synthesis and/or possible instability of Sc_3InB structure seems to be in line with unstable phonon branches, which were detected in our phonon calculations. Also it is known, that cubic Sc_3In structure is only stable when synthesized under high pressure (6.5 GPa⁵³), so maybe similar attempts should be undertaken in the boron-stabilized perovskite structure. Further experimental study is required to verify whether Sc_3InB is really a superconductor.

* Corresponding author, email: tobola@ftj.agh.edu.pl

¹ B. Wiendlocha, J. Tobola, S. Kaprzyk, D. Fruchart, and J. Marcus, The European Conference Physics of Magnetism'05, 24-27.06.2005, Poznan, Poland. Preprint: cond-mat/0506793.

² T. He, Q. Huang, A. P. Ramirez, Y. Wang, K. A. Regan, N. Rogado, M. A. Hayward, M. K. Haas, J. S. Slusky, K. Inumara, et al., *Nature* **411**, 54 (2001).

³ H. Rosner, R. Weht, M. D. Johannes, W. E. Pickett, and E. Tosatti, *Phys. Rev. Lett.* **88**, 27001 (2002).

⁴ P. M. Singer, T. Imai, T. He, M. A. Hayward, and R. J. Cava, *Phys. Rev. Lett.* **87**, 257601 (2001).

⁵ J. Y. Lin, P. L. Ho, H. L. Huang, P. H. Lin, Y. L. Zhang, R. C. Yu, C. Q. Jin, and H. D. Yang, *Phys. Rev. B* **67**, 52501 (2003).

⁶ T. G. Kumary, J. Janaki, A. Mani, S. M. Jaya, V. S. Sastry, Y. Hariharan, T. S. Radhakrishnan, and M. C. Valsakumar, *Phys. Rev. B* **66**, 64510 (2002).

⁷ G. Garbarino, M. Monteverde, M. Nez-Regueiro, C. Acha, R. Weht, T. He, K. A. Regan, N. Rogado, M. Hayward, and R. J. Cava, *Physica C* **408**, 754 (2004).

⁸ Z. Q. Mao, M. M. Rosario, K. D. Nelson, K. Wu, I. G. Deac, P. Schiffer, Y. Liuy, T. He, K. A. Regan, and R. J. Cava, *Phys. Rev. B* **67**, 94502 (2003).

⁹ R. Prozorov, A. Snezhko, T. He, and R. J. Cava, *Phys. Rev. B* **68**, 180502 (2003).

¹⁰ A. Y. Ignatov, S. Y. Savrasov, and T. A. Tyson, *Phys. Rev. B* **68**, 220504 (2003).

¹¹ R. Heid, B. Renker, H. Schober, P. Adelmann, D. Ernst, and K. P. Bohnen, *Phys. Rev. B* **69**, 92511 (2004).

¹² S. Y. Li, W. Q. Mo, M. Yu, W. Zheng, C. H. Wang, Y. M. Xiong, R. Fan, H. S. Yang, B. M. Wu, L. Z. Cao, et al., *Phys. Rev. B* **65**, 64534 (2002).

¹³ R. E. Schaak, M. Avdeev, W.-L. Lee, G. Lawes, H. W. Zandbergen, J. D. Jorgensen, N. P. Ong, A. P. Ramirez, and R. J. Cava, *J. Solid State Chem.* **177**, 1244 (2004).

¹⁴ M.-S. Park, J. Giim, S.-H. Park, Y. W. Lee, S. I. Lee, and E. J. Choi, *Supercond. Sci. Technol.* **17**, 274 (2004).

¹⁵ M. D. Johannes and W. E. Pickett, *Phys. Rev. B* **70**, 060507 (2004).

¹⁶ H. Holleck, *J. Less Common Met.* **52**, 167 (1977).

¹⁷ B. T. Matthias, A. M. Clogston, H. J. Williams, E. Corenzwit, and R. C. Sherwood, *Phys. Rev. Lett.* **7**, 7 (1961).

¹⁸ ed. by, W. H. Butler, P. Dederichs, A. Gonis, and R. Weaver, *Chapter III, in: Applications of Multiple Scattering Theory to Materials Science*, vol. 253 (MRS Symposia Proceedings, MRS Pittsburgh, 1992).

¹⁹ S. B. der Kellen, Y. Oh, E. Badralexe, and A. J. Freeman, *Phys. Rev. B* **51**, 9560 (1995).

²⁰ T. Stopa, S. Kaprzyk, and J. Tobola, *J. Phys.: Condens. Matter* **16**, 4921 (2004).

²¹ W. L. McMillan, *Phys. Rev.* **167**, 331 (1968).

²² J. J. Hopfield, *Phys. Rev.* **186**, 443 (1969).

²³ G. D. Gaspari and B. L. Gyorffy, *Phys. Rev. Lett.* **28**, 801 (1972).

²⁴ W. E. Pickett, *Phys. Rev. B* **25**, 745 (1982).

²⁵ S. Baroni, A. D. Corso, S. de Gironcoli, and P. Giannozzi, www.pwscf.org.

²⁶ T. Amos, Q. Huang, J. Lynn, T. He, and R. Cava, *Solid State Comm.* **121**, 73 (2002).

²⁷ S. B. Dugdale and T. Jarlborg, *Phys. Rev. B* **64**, 100508 (2001).

²⁸ A. Szajek, *J. Phys.: Condens. Matter* **13**, 595 (2001).

²⁹ S. Baroni, A. D. Corso, S. de Gironcoli, and P. Giannozzi, *Rev. Mod. Phys.* **73**, 515 (2001).

³⁰ D. Vanderbilt, *Phys. Rev. B* **41**, 7892 (1990).

³¹ M. Methfessel and A. T. Paxton, *Phys. Rev. B* **40**, 3616 (1989).

³² A. Y. Ignatov, L. Dieng, T. Tyson, T. He, and R. Cava, *Phys. Rev. B* **67**, 064509 (2003).

³³ I. I. Mazin, S. N. Rashkeev, and S. Y. Savrasov, *Phys. Rev. B* **42**, 366 (1990).

³⁴ A. D. Zdetsis, E. N. Economou, and D. A. Papaconstantopoulos, *Phys. Rev. B* **24**, 3115 (1981).

³⁵ W. H. Butler, J. J. Olson, J. S. Faulkner, and B. L. Gyorffy, *Phys. Rev. B* **14**, 3823 (1976).

³⁶ W. H. Butler, *Phys. Rev. B* **15**, 5267 (1977).

³⁷ S. Y. Savrasov and D. Y. Savrasov, *Phys. Rev. B* **54**, 16487 (1996).

³⁸ D. A. Papaconstantopoulos, L. L. Boyer, B. M. Klein, A. R. Williams, V. L. Moruzzi, and J. F. Janak, *Phys. Rev. B* **15**, 4221 (1977).

³⁹ S. S. Rajput, R. Prasad, R. M. Singru, S. Kaprzyk, and A. Bansil, *J. Phys.: Condens. Matter* **8**, 2929 (1996).

⁴⁰ B. M. Klein, L. L. Boyer, and D. A. Papaconstantopoulos, *Phys. Rev. Lett.* **42**, 530 (1979).

⁴¹ B. M. Klein and D. A. Papaconstantopoulos, *Phys. Rev. Lett.* **32**, 1193 (1974).

⁴² S. V. Halilov, D. J. Singh, and D. A. Papaconstantopoulos, *Phys. Rev. B* **65**, 174519 (2002).

⁴³ W. E. Pickett and D. J. Singh, *Phys. Rev. Lett.* **72**, 3702 (1994).

⁴⁴ D. A. Papaconstantopoulos and B. M. Klein, *Phys. Rev. Lett.* **35**, 110 (1975).

⁴⁵ J. Kortus, I. I. Mazin, K. D. Belashenko, V. P. Antropov, and L. L. Boyer, *Phys. Rev. Lett.* **86**, 4656 (2001).

⁴⁶ W. E. Pickett, *Rev. Mod. Phys.* **61**, 433 (1989).

⁴⁷ H. J. Choi, D. Roundy, H. Sun, M. L. Cohen, and S. G. Louie, *Nature* **418**, 758 (2002).

⁴⁸ A. Floris, G. Profeta, N. N. Lathiotakis, M. Luders, M. A. L. Marques, C. Franchini, E. K. U. Gross, A. Continenza, and S. Massidda, *Phys. Rev. Lett.* **94**, 37004 (2005).

⁴⁹ T. Klimczuk and R. J. Cava, *Phys. Rev. B* **70**, 212514 (2004).

⁵⁰ A. Bansil, S. Kaprzyk, P. E. Mijnarends, and J. Tobola, *Phys. Rev. B* **60**, 13396 (1999).

⁵¹ Z. A. Ren, G. C. Che, S. L. Jia, H. Chen, Y. M. Ni, G. D. Liu, and Z. X. Zhao, *Physica C* **371**, 1 (2002).

⁵² V. B. Compton and B. T. Matthias, *Acta Cryst.* **15**, 94 (1962).

⁵³ A. Palenzona, P. Manfrinetti, and R. Palenzona, *J. All. Compd.* **15**, 94 (1996).

⁵⁴ A. Aguayo and D. J. Singh, *Phys. Rev. B* **66**, 20401 (2002).

⁵⁵ A. Aguayo, I. I. Mazin, and D. J. Singh, *Phys. Rev. Lett.* **92**, 147201 (2004).

⁵⁶ A. Kolodziejczyk and J. Spalek, *J. Phys. F* **14**, 1277 (1984).

⁵⁷ C. Pfeiderer, *Nature* **412**, 58 (2001).

⁵⁸ J. H. Shim, S. K. Kwon, and B. I. Min, *Phys. Rev. B* **64**, 180510 (2001).

⁵⁹ definition of the n -th frequency moment, basing on Eliashberg function $\alpha^2 F(\omega)$: $\langle \omega^n \rangle = \int \omega^{n-1} \alpha^2 F(\omega) d\omega / \int \omega^{-1} \alpha^2 F(\omega) d\omega \simeq$

$\int \omega^{n-1} F(\omega) d\omega / \int \omega^{-1} F(\omega) d\omega$, if $\alpha^2 \simeq const.$
⁶⁰ We used $\langle \omega \rangle / 1.2$ with $\langle \omega \rangle = 19.5$ meV instead of $\omega_D / 1.45$ in McMillan formula in practical computations.

⁶¹ For MgNi₃ we took lattice constant smaller about 2.5%:
7.206 Bohr in MgCNi₃, 7.050 in MgNi₃.